Optimized Design of Subsonic Lifting Surfaces

JAMES W. MCDONALD* AND JAMES R. STEVENS†
Northrop Corporation, Hawthorne, Calif.

A procedure, based on the kernel function method of linearized lifting-surface theory, for designing and analyzing wings in steady, low-speed flight is described. Optimized smooth surfaces were designed using this method for high lift and cruise operations. The optimization is obtained by constraining the spanwise lift distribution to be elliptic. The theoretically predicted performance of the lifting surfaces was compared to wind-tunnel data. It can be inferred from the results that if high lift is the prime requirement, then it is preferable to design an optimized, smooth, high lift wing and deflect the flaps to produce a kinky cruise configuration. The application of the procedure indicates that it reduces significantly the time and expense required to generate a wing having desired characteristics.

Nomenclature

a = coefficients in the pressure loading series
A = aspect ratio
A_j = coefficient in the equation describing the spanwise variation of c for wing panel j [Eq. (24)]
$[A]$ = vector composed of the elements a
b = wing span
B_j = coefficient in the equation describing the spanwise variation of c for wing panel j [Eq. (24)]
c = local wing chord
$\bar{c}$ = mean aerodynamic chord
c_a = average wing chord
C_{Di} = induced drag coefficient
c_0 = root chord
C_j = coefficient in equation giving the spanwise variation of $(\xi_L - \xi_0)$ for wing panel j[Eq. (25)]
C_l = local lift coefficient
C_L = total lift coefficient
C_m = local moment coefficient referred to the axis $\xi = \xi_0$
C_M = total moment coefficient referred to one quarter of the mean aerodynamic chord
d = integral of pressure loading modes over the wing planform [see Eqs. (9) and (11)]
D = total drag
$[D]$ = matrix composed of the elements d
D_j = coefficient in the equation giving the spanwise variation of $(\xi_L - \xi_0)$ for wing panel j [Eq. (25)]
e = wing efficiency factor [Eq. (41)]
f = chordwise loading mode related to a deflected flap
G = coefficient defined by Eq. (34)
H = coefficient defined by Eq. (21)
I = coefficient defined by Eq. (35)
J = number of wing panels
K = kernel function [Eq. (2)]
l = chordwise loading modes related to camber and twist
L = total lift
$L(\theta,\eta)$ = chordwise loading series
M = number of spanwise loading modes
N = number of l chordwise loading modes
N_f = number of deflected flaps
p_r = pressure loading distribution nondimensionalized by $\frac{1}{2}\rho V^2$
P = coefficient defined by Eq. (27)
R = coefficient defined by Eq. (26)
$R_{\bar{c}}$ = Reynolds number referred to $\bar{c}$
s = b/c_0
V = freestream velocity
w = slope of mean wing surface or downwash velocity reduced by V
$[W]$ = vector composed of elements w
x = dimensionless chordwise variable referred to $c_0/2$ and aligned with V
y = dimensionless spanwise variable referred to $b/2$
α = angle of attack
β = Prandtl-Glauert compressibility correction
Γ = circulation
δ = flap deflection angle
η = dimensionless spanwise variable referred to $b/2$
θ = angular chordwise variable defined by Eq. (8)
κ = modified kernel function [Eq. (10)]
λ = taper ratio
Λ = sweepback angle
ξ = dimensionless chordwise variable referred to $c_0/2$
ξ_0 = moment axis
ρ = fluid density
ϕ = angular spanwise variable defined by Eq. (28)
χ = coefficient defined by Eq. (16)
ω = downwash velocity defined by Eq. (30)

Subscripts

eff = effective value for envelope
F = trailing edge flap
L = leading edge
N = leading edge or nose flap
t = flap related variable
T = trailing edge

Indices

j = panel index
m = spanwise mode index
n = chordwise mode index
p = $2(m - 1)$
t = flap mode index
γ = $2(\nu - 1)$
μ = $2(\sigma - 1)$
ν = index equivalent to m
σ = index equivalent to m

Received July 30, 1969; revision received December 31, 1969. This research was sponsored by the Department of the Navy, Bureau of Naval Weapons, under Contracts NOw-63-0726-c and NOw-65-0380-c, with O. Seidman as Technical Monitor.

* Senior Engineer, Aircraft Division; presently Graduate Student, School of Engineering and Applied Science, University of California, Los Angeles, Calif.

† Member of Technical Management, Aircraft Division. Member AIAA.

Introduction

THE development of a wing for a required subsonic mission is an ever present problem, especially for high lift. In the past, the initial design of lifting surfaces has been based mainly on empirical and strip methods. The initial configuration is wind-tunnel tested and intuitive or empirical modifications are made. This process, test and modify, is repeated until a suitable final configuration is obtained. It is obvious that this approach is both costly and time consuming. In order to reduce this expense and improve the wing performance, it is desirable to have a design procedure which accounts for plan-

form or three-dimensional effects. This has been achieved by the use of lifting-surface theory. This new procedure has been applied to the design of both high lift and cruise wings. The performance of these surfaces was compared with that of other wings using various high lift devices. The reasons for doing this were to examine the limit of applicability of planar lifting-surface theory to high lift design, and to determine the performance improvement of high lift wings designed by this method.

Theoretical Development

Lifting-surface theory relates the slope distribution of the mean surface of the wing to the pressure loading distribution by the following integral equation[1]:

$$w(x,y) = \frac{1}{8}\rho b c_0 V \int_{-1}^{+1}\int_{\xi_L(\eta)}^{\xi_T(\eta)} p_r(\xi,\eta) K d\xi d\eta \qquad (1)$$

where

$$K = \frac{1}{\pi\rho V c_0^2 s^2 (y-\eta)^2}\left\{1 + \frac{x-\xi}{[(x-\xi)^2 + \beta^2 s^2 (y-\eta)^2]^{1/2}}\right\} \qquad (2)$$

The kernel function K may be interpreted as an influence coefficient which gives the downwash induced at the point $(c_0x/2,y)$ by the loading on the elemental area at $(c_0\xi/2,\eta)$ (Fig. 1). Thus, the integral over the planform gives the downwash induced at the collocation point $(c_0x/2,y)$ by the entire loading distribution. It should be noted that the semispan in Fig. 1 has been normalized to unity. Equation (1) was solved by Watkins et al.,[1] using the method of undetermined coefficients. That is, a series expansion similar to the following was assumed to represent the pressure loading:

$$p_r(\theta,\eta) = 8\pi(b/c)(1-\eta^2)^{1/2} L(\theta,\eta) \qquad (3)$$

where

$$L(\theta,\eta) = \sum_{n=0}^{N-1}\sum_{m=1}^{M} a_{np}\eta^p l_n(\theta) + \sum_{t=1}^{N_f}\sum_{m=1}^{M} a_{tp}\eta^p f_t(\theta) \qquad (4)$$

$$l_n(\theta) = \begin{cases}\cot(\theta/2), & n = 0\\ (4/2^{2n})\sin n\theta, & n > 0\end{cases} \qquad (5)$$

$$f_t(\theta) = \frac{1}{\gamma}\log\left|\frac{\sin\frac{1}{2}(\theta_t+\theta)}{\sin\frac{1}{2}(\theta_t-\theta)}\right| \qquad (6)$$

and

$$p = 2(m-1) \qquad (7)$$

$$\xi = \tfrac{1}{2}(\xi_L + \xi_T) - (c/c_0)\cos\theta \qquad (8)$$

The first series in Eq. (4) expresses the loading caused by twist and camber, and the second series represents the loading produced by deflected flaps. The chordwise functions $l_n(\theta)$ enable the loading to have a leading edge singularity, and satisfy the Kutta condition. The cotangent mode is the principal term representing the additional loading, and the sine modes mainly express the loading caused by camber. The chordwise flap mode[2] $f_t(\theta)$ contains a singularity at the position tion of the flap hinge line which is denoted by θ_t.

Substituting Eqs. (3) and (2) into Eq. (1) yields

$$w(x,y) = \sum_{n=0}^{N-1}\sum_{m=1}^{M} a_{np}\int_{-1}^{+1}\int_{0}^{\pi} l_n(\theta)\eta^p \kappa \sin\theta d\theta d\eta + \sum_{t=1}^{N_f}\sum_{m=1}^{M} a_{tp}\int_{-1}^{+1}\int_{0}^{\pi} f_t(\theta)\eta^p \kappa \sin\theta d\theta d\eta \qquad (9)$$

where

$$\kappa = \pi\rho V c_0^2 s^2 (1-\eta^2)^{1/2} K \qquad (10)$$

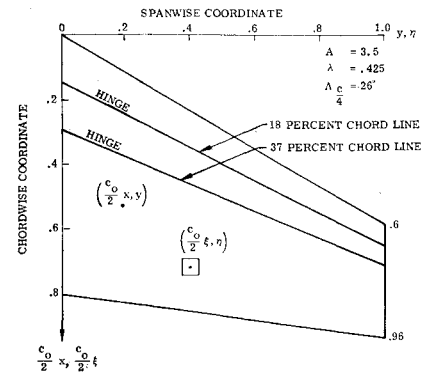

Fig. 1 Wing planform showing flap arrangement.

Performing the quadrature[1,3,4] indicated in Eq. (9) results in

$$w(x,y) = \sum_{n=0}^{N=1}\sum_{m=1}^{M} a_{np}d_{np} + \sum_{t=1}^{N_f}\sum_{m=1}^{M} a_{tp}d_{tp} \qquad (11)$$

where d_{np} and d_{tp} are the values obtained for the corresponding integrals in Eq. (9). Repeating this calculation for several collocation points gives a set of Eq. (11) which may be expressed in matrix form:

$$[W] = [D][A] \qquad (12)$$

Inverting Eq. (12) gives

$$[A] = [D]^{-1}[W] \qquad (13)$$

A computer program[3,4] was developed to generate and solve Eqs. (12) and (13). A least squares solution was used. For a given planform and Mach number, Eq. (13) was solved to give the pressure loading and aerodynamic coefficients for various mean surface shapes and angles of attack. The analysis procedure was verified using planforms which provided a wide range in aspect ratio, taper ratio, and sweep back.[3] The agreement between wind-tunnel data and the theoretical predictions was good. The solution to Eq. (12) is presented in the the section entitled "The Design Procedure."

Aerodynamic Coefficients

In the derivation of the aerodynamic coefficient equations it was assumed that the planform could be approximated by a set of panels with straight leading and trailing edges. It was also assumed that the flaps were full span and their hinge lines were colinear with the wing element lines.

1) Lift coefficient:

Defining the local lift coefficient as

$$C_l(\eta) = \frac{c_0}{2c}\int_{\xi_L(\eta)}^{\xi_T(\eta)} p_r(\xi,\eta)d\xi \qquad (14)$$

and integrating gives

$$C_l(\eta) = \frac{4\pi^2 b}{c}(1-\eta^2)^{1/2}\sum_{m=1}^{M}\chi_p\eta^p \qquad (15)$$

where

$$\chi_p = a_{0p} + \frac{1}{2}a_{1p} + \frac{1}{\pi}\sum_{t=1}^{N_f} a_{tp}\sin\theta_t \qquad (16)$$

The total lift coefficient is then given as

$$C_L = \frac{1}{2}\int_{-1}^{+1}\frac{C_l(\eta)c}{c_a}d\eta = \qquad (17)$$

$$\frac{2\pi^2 b}{c}\left[\frac{\pi}{2}\chi_0 + \frac{\pi}{8}\chi_2 + \frac{\pi}{8}\sum_{m=3}^{M}\frac{(p-1)(p-3)\ldots 3}{(p+2)p\ldots 6}\chi_p\right] \qquad (18)$$

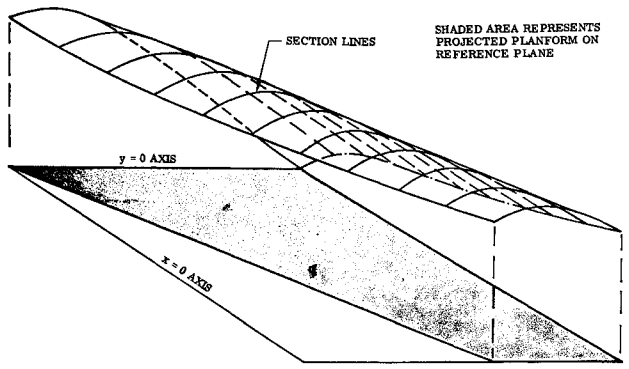

Fig. 2 Mean surface of high lift wing.

2) Moment coefficient:

The local moment coefficient about the axis $\xi = \xi_0$ is defined as

$$C_m(\eta) = -\frac{c_0^2}{4c^2}\int_{\xi_L(\eta)}^{\xi_T(\eta)} p_r(\xi,\eta)(\xi - \xi_0)d\xi \tag{19}$$

$$C_m(\eta) = -\frac{2\pi^2 b}{c^2}(1-\eta^2)^{1/2}\times \left[c\sum_{m=1}^{M} H_p\eta^p + c_0(\xi_L - \xi_0)\sum_{m=1}^{M}\chi_p\eta^p\right] \tag{20}$$

where

$$H_p = \frac{1}{2}a_{0p} + \frac{1}{2}a_{1p} - \frac{1}{16}a_{2p} + \frac{1}{\pi}\sum_{t=1}^{N_f} a_{tp}\sin\theta_t \tag{21}$$

Defining the total moment coefficient as

$$C_M = \frac{1}{2}\int_{-1}^{+1}\frac{c^2 C_m(\eta)}{c_a\bar{c}}\,d\eta \tag{22}$$

where ξ_0 now equals the location of the quarter chord station of the mean aerodynamic chord. Integrating yields

$$C_M = -\frac{4\pi^2 b}{c_a\bar{c}}\sum_{m=1}^{M}\sum_{j=1}^{J}\left[H_p(A_jR_p + B_jP_p) + \frac{c_0}{2}\chi_p(C_jR_p + D_jP_p)\right] \tag{23}$$

The subscript j designates a particular wing panel and the geometry of the panel is given by the linear equations

$$\tfrac{1}{2}c_j(\eta) = A_j + B_j\eta, \quad \eta_{j-1} \le \eta \le \eta_j \tag{24}$$

$$\xi_L(\eta) - \xi_0 = C_j + D_j\eta, \quad \eta_{j-1} \le \eta \le \eta_j \tag{25}$$

The symbol η_j denotes the spanwise boundaries of the panels, i.e., $\eta_0 = 0$ and $\eta_j = 1$. Also, we have

$$R_p = \tfrac{1}{2}(\phi_j - \phi_{j-1}) - \tfrac{1}{4}(\sin 2\phi_{j-1} - \sin 2\phi_j), \quad p = 0$$

$$R_p = [1/(p+2)](\cos^{p-1}\phi_{j-1}\sin^3\phi_{j-1} - \cos^{p-1}\phi_j \times \sin^3\phi_j) + [p - 1/p + 2]R_{p-2}, \quad p \ge 2 \tag{26}$$

$$P_p = \tfrac{1}{3}(\sin^3\phi_{j-1} - \sin^3\phi_j), \quad p = 0$$

$$P_p = [1/(p+3)](\cos^p\phi_{j-1}\sin^3\phi_{j-1} - \cos^p\phi_j\sin^3\phi_j) + [p/(p+3)]P_{p-2}, \quad p \ge 2 \tag{27}$$

where ϕ is related to η by

$$\eta = \cos\phi \tag{28}$$

3) Drag coefficient

The over-all induced drag coefficient is defined by

$$C_{Di} = \frac{1}{c_a V^2}\int_{-1}^{+1}\omega(y)\Gamma(y)dy \tag{29}$$

where

$$\omega(y) = \frac{1}{2\pi b}\int_{-1}^{+1}\frac{[d\Gamma(\eta)/d\eta]}{(y-\eta)}\,d\eta \tag{30}$$

$$\Gamma(\eta) = \frac{cV}{4}\int_0^{\pi} p_r(\theta,\eta)\sin\theta d\theta \tag{31}$$

Substituting for p_r and carrying out the quadrature yields

$$C_{Di} = \frac{2\pi^4 b}{c_a}\sum_{\sigma=1}^{M}\sum_{\gamma=1}^{\sigma}\sum_{m=1}^{M} I_\gamma(\mu)\chi_\mu\chi_p G_{\mu-\gamma+p} \tag{32}$$

where

$$\gamma = 2(\nu - 1), \quad \mu = 2(\sigma - 1) \tag{33}$$

and

$$G_0 = \pi/2, \quad G_2 = \pi/8, \quad G_p = (p-1)(p-3)\ldots 3/(p+2)p\ldots 6\pi/8 \tag{34}$$

$$I_\gamma(\mu) = \mu + 1, \ \gamma = 0$$

$$I_\gamma(\mu) = \tfrac{1}{2}(1-\mu), \ \gamma = 2$$

$$I_\gamma(\mu) = \frac{(\gamma-3)(\gamma-5)\ldots(1)}{(\gamma-2)(\gamma-4)\ldots(2)}\frac{(\gamma-\mu-1)}{\gamma}, \quad \gamma \ge 4 \tag{35}$$

Design Procedure

There are two design options available: the first determines the slope distribution required to produce a specified loading distribution, and the second calculates the mean surface shape that minimizes the induced drag for specified total lift and moment coefficients. In the first option, the matrix A in Eq. (12) is determined by a least squares fit of the specified loading. This is described in Refs. 4 and 5.

The second option, which optimizes the loading, is certainly more important. Flap loading modes are not considered in the design procedure since it would be impractical, although feasible. The loading is optimized by constraining the spanwise lift distribution to be elliptic as determined by a variational analysis. The constraint is obtained by discarding the spanwise loading terms corresponding to $m > 1$. Thus,

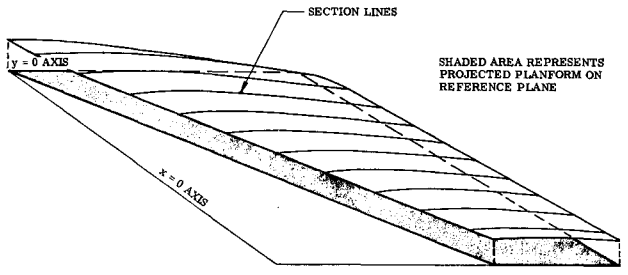

Fig. 3 Mean surface of cruise wing.

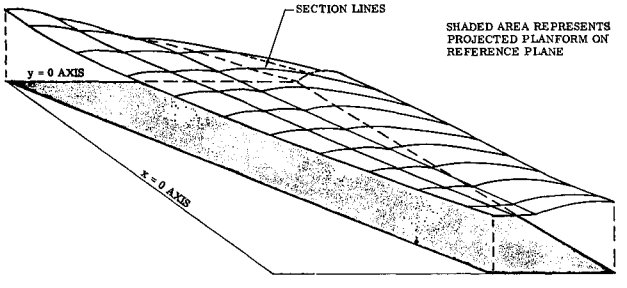

Fig. 4 Mean surface of approximate cruise wing.

Eq. (15) becomes

$$C_l(\eta) = (4\pi^2 b/c)(1 - \eta^2)^{1/2}\chi_0 \tag{36}$$

where

$$\chi_0 = a_{00} + \tfrac{1}{2} a_{10}$$

and (37)

$$C_L = (\pi^3 b/c_a)(a_{00} + \tfrac{1}{2} a_{10})$$

The resulting series describing the optimized loading distribution is

$$p_r(\theta,\eta) = \frac{8\pi b}{c}(1 - \eta^2)^{1/2} \times \left(a_{00}\cot\frac{\theta}{2} + a_{10}\sin\theta + \frac{1}{4}\sum_{m=1}^{M} a_{2p}\eta^p \sin 2\theta\right) \tag{38}$$

The chordwise modes for $n > 2$ are omitted since they do not contribute to the lift and moment coefficients. The spanwise variation in the mode $n = 2$ is not restricted since it only contributes to the moment coefficients.

The resulting equation for the total moment coefficient is

$$C_M = -\frac{2\pi^2 b}{c_a \bar{c}}\sum_{j=1}^{J}\left\{a_{00}[(A_jR_0 + B_jP_0) + c_0(C_jR_0 + D_jP_0)] + a_{10}\left[(A_jR_0 + B_jP_0) + \frac{c_0}{2}(C_jR_0 + D_jP_0)\right] - \frac{1}{8}\sum_{m=1}^{M} a_{2p}(A_jR_p + B_jP_p)\right\} \tag{39}$$

Equations (37) and (39) are used to obtain the coefficients for $[A]$. For the situation where only the basic type of loading is wanted, the coefficient a_{00} is made zero. This leaves $M + 1$ of the a_{np} coefficients to be determined. Since only two equations are available this means that $M - 1$ may be specified arbitrarily. However, one has little physical understanding from which to specify the coefficients. Thus, it has been the practice to set

$$a_{2p} = 0, \quad p > 0 \tag{40}$$

and solve for a_{10} and a_{20}. Also, it is considered that zero leading edge load reduces adverse real fluid effects such as separation.

Designed Wings

Four wings were designed: 1) a smooth high lift wing (Fig. 2), 2) a smooth cruise wing (Fig. 3), 3) an approximation of the cruise wing by the high lift wing using flap deflections (Fig. 4), and 4) an approximation of the high lift wing by the cruise wing using flap deflections (Fig. 5). Lift and moment coefficients of 2.0 and -0.3, respectively, were selected for the high lift wing. This moment coefficient was used since it resulted in a pressure loading distribution with a linear chordwise variation over the aft portion of the wing. It was considered that this would reduce flow separation. However, it was found that the spanwise curvature of the surface at the root was extremely large, and therefore impractical. Linear extrapolations were made of the mean surface along element lines from several spanwise tangent points until one was obtained which provided a practical root shape and aerodynamic coefficients near the original values. An isometric view of the final mean surface is shown in Fig. 2. The sectional mean lines have been aligned at the 25% chord station.

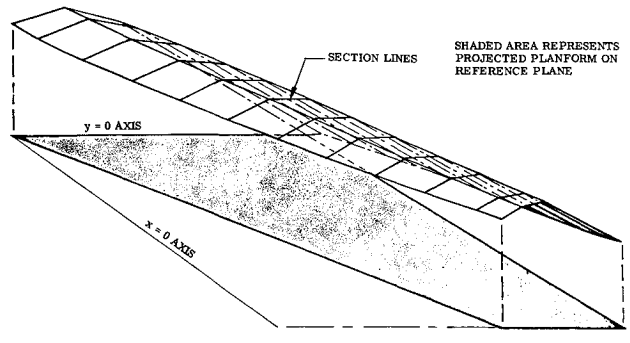

Fig. 5 Mean surface of approximate high lift wing.

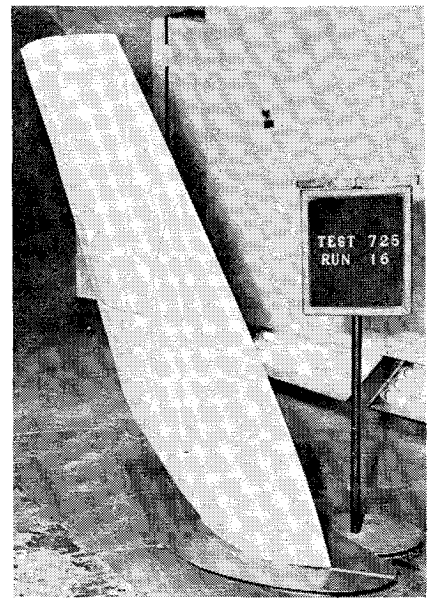

Fig. 6 Downstream view of upper surface of high lift wing model.

The cruise wing was designed for a lift coefficient of 0.3 and a moment coefficient of -0.045. The mean surface obtained is shown in Fig. 3 with the sectional mean lines aligned at 25% chord.

The aft region of the smooth wings were virtually flat. Therefore, only the forward portions needed to be modified to give the approximate wings. The flap hinge lines and planform used for the wings are shown in Fig. 1. This configuration was selected since it was fairly representative of current naval aircraft. The hinge lines coincide with the 18 and 37% chord element lines. The flap deflections were determined so that 1) the magnitude and spanwise variation of the local ideal angle of attack was minimized, 2) the differences between the slope distributions of the approximate and smooth wings were minimized, and 3) the resulting design was practical. The resulting flap deflections had a linear spanwise variation. The approximate wings are shown in Figs. 4 and 5.

Models with a 4-ft semispan were constructed with a NACA 64 A 004 airfoil superimposed on the mean camber lines. This airfoil, having a maximum thickness of 4%, was selected in order to minimize thickness effects.

Test Results

The models were tested in the Northrop low-speed wind tunnel (Fig. 6). The results for the high lift wing are shown in Fig. 7. The solid lines represent the calculations of the analysis procedure. The performance of this wing is excellent as shown in later comparisons, even though the agreement between theory and test is not altogether satisfactory. The parasite drag is seen to decrease as the design point ($C_L = 1.945$, $C_M = -0.319$) is approached. The lift curve slope is adequately predicted, and the design moment is approached near the design point. The maximum lift obtained was 1.8 at 4° angle of attack. This is 7.5% less than the design coefficient. Near the design point, the flow over the surface of the

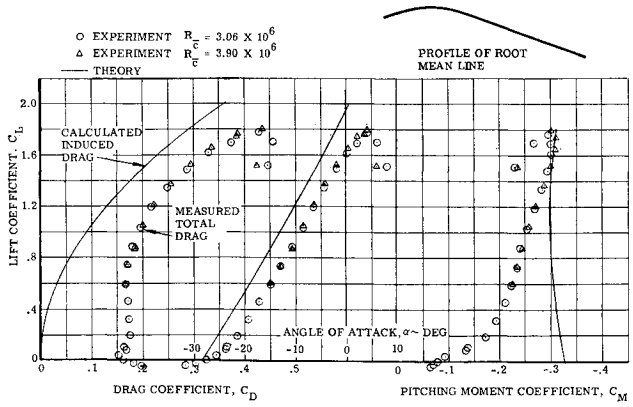

Fig. 7 Comparison of theory and experiment, wing 1 fixed transition.

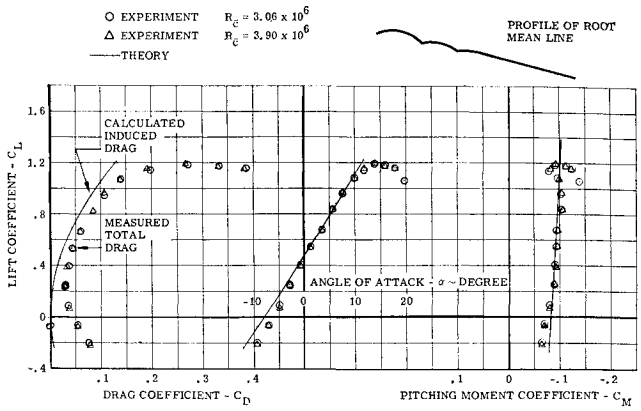

Fig. 9 Comparison of theory and experiment, wing 3 fixed transition.

wing was parallel to the mainstream, as indicated by tufts. This is probably the reason why the flow was not separated, even though the wing had a large negative slope (−0.8) over the aft portion.

Figure 8 compares the calculated and measured coefficients for the cruise wing. The agreement is good, however the lift is slightly overestimated. The measured lift to drag ratio near the design point ($C_L = 0.3, C_M = -0.045$) was 17 to 1.

The comparison for the approximate cruise wing was also good (Fig. 9). Note the excellent agreement between the measured and calculated moments. This indicates that the loading distribution is well predicted in spite of the kinky shape.

The agreement for the approximate high lift wing is poor because of flow separation at the hinge lines (Fig. 10). Separation occurred at the aft hinge lines at approximately −14° angle of attack and at the forward hinge line at 0°. This may be seen from the discontinuities in the trend of the test points.

Performance Evaluation

The performance of the wings was evaluated in terms of their lift to drag ratios. The envelope of the drag polars for a wing with various camber distributions or high lift devices can be given by

$$C_D = C_{D_{o_{\text{eff}}}} + (C_L^2/\pi A e_{\text{eff}}) \tag{41}$$

The lift to drag ratio of the envelope is then

$$L/D = [C_L/C_{D_{o_{\text{eff}}}} + (C_L^2/\pi A e_{\text{eff}})] \tag{42}$$

Dividing Eq. (42) by $A^{1/2}$ gives

$$L/D/A^{1/2} = C_L/A^{1/2}/[C_{D_{o_{\text{eff}}}} + (1/\pi e_{\text{eff}})(C_L/A^{1/2})^2] \tag{43}$$

Equation (43) is used to compare wings with various aspect ratios and high lift devices. The parameter $(L/D)/A^{1/2}$ is termed the "reduced lift-drag ratio" and $C_L/A^{1/2}$ is called the "reduced lift coefficient." The expression then provides a display on a single graph of $(L/D)/A^{1/2}$ vs $C_L/A^{1/2}$ which is parametric in $C_{D_{o_{\text{eff}}}}$ and e_{eff}. The upper limit of performance would correspond to $C_{D_{o_{\text{eff}}}} = 0$ and $e_{\text{eff}} = 1.0$ in which case Eq. (43) reduces to

$$(L/D/A^{1/2})_{\text{upper limit}} = \pi/C_L/A^{1/2} \tag{44}$$

The degree to which a given wing approaches the upper limit can be expressed as

$$(L/D/A^{1/2})_{\text{actual}}/(L/D/A^{1/2})_{\text{upper limit}} = [C_L/C_D/A^{1/2}]/[\pi/(C_L/A^{1/2})] = C_L^2/\pi A C_D$$

As the lift coefficient increases to high values, this ratio approaches the conventional span efficiency factor. The performance of the four wings is presented in Fig. 11. The envelope of the test data indicates that a wing can be designed, using this method, to have a performance at any point on the curve up to $C_L \simeq A^{1/2}$.

Figure 12 compares the present test envelope with wings using high lift devices tested by the NACA. The evaluation was actually more extensive than shown.[4] The high lift devices selected for this comparison are leading edge droop and plain trailing edge flaps, since these correspond with the geometry of the approximate wings. It is to be noted that the approximate wings were not obtained by deflecting movable flaps, but were constructed with a fixed design shape. The hinge lines were actually lines of discontinuity in the chordwise slope distribution. Figure 12 and the comparisons not

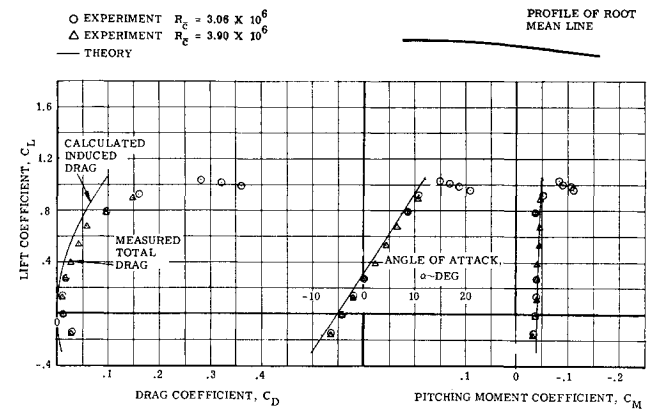

Fig. 8 Comparison of theory and experiment, wing 2 fixed transition.

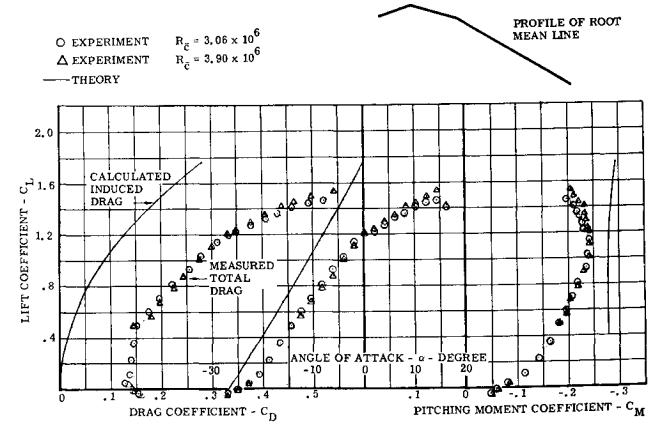

Fig. 10 Comparison of theory and experiment, wing 4 fixed transition.

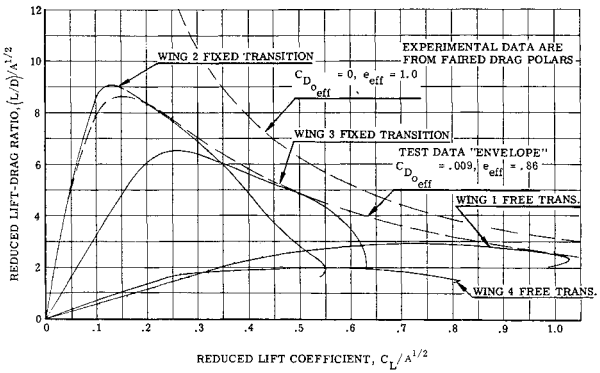

Fig. 11 Comparison of reduced lift-drag ratios.

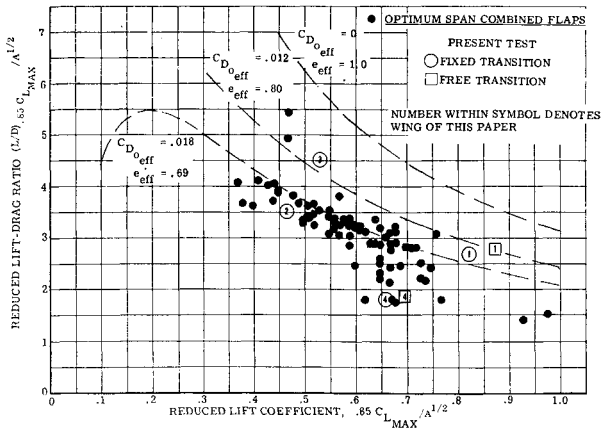

Fig. 13 Reduced lift-drag ratio at 85% maximum lift.

shown here indicate the designed wings had performance as good as or better than the wings using high lift devices.

The high lift performance comparison is summarized in Fig. 13. Here, several wings tested by the NACA are compared at 85% of maximum C_L. Optimum span high lift flaps are those devices which provide the highest maximum lift and lift to drag ratios (not simultaneously). Again, the smooth high lift wing has superior performance. Also, the approximate cruise wing has better performance than the other wings having the same reduced lift coefficient.

Conclusions

The application of planar lifting-surface theory to high lift design can produce a wing with performance superior to similar wings using high lift devices. The results indicated that the method generated excellent cruise wings and provided good predictions of their performance.

However, it may be concluded that planar lifting-surface theory does not accurately predict the characteristics of a high lift wing. In results not shown here,[5] the over-all magnitude of the pressure loading distribution was satisfactorily predicted but the distribution was off somewhat. This difference may be reduced by using a nonplanar kernel function, although this may be regarded as contradictory to the linearization. Also, a nonplanar kernel would result in an iterative design procedure. The comparisons obtained in Fig. 13 indicate that if maximum lift is the principle requirement, then it is better to design for high lift and deflect the flaps to give a kinky cruise configuration.

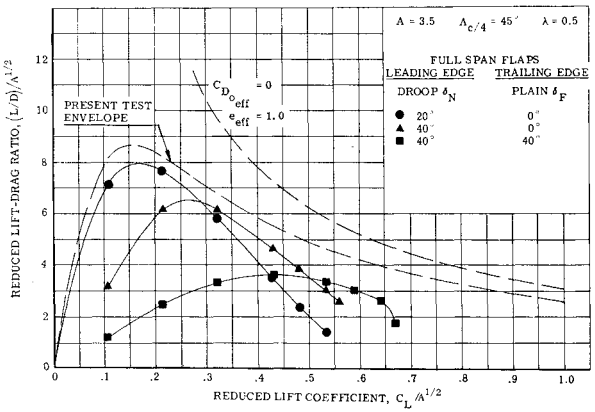

Fig. 12 Reduced lift-drag ratio—comparison.

References

[1] Watkins, C. E., Woolston, D. S., and Cunningham, H. J., "A Systematic Kernel Function Procedure for Determining Aerodynamic Forces on Oscillating or Steady Finite Wings at Subsonic Speeds," TR 48, 1958, N SA.

[2] Allen, H. J., "Calculations of the Chordwise Load Distribution over Airfoil Sections with Plain, Slit, or Serially Hinged Trailing-Edge Flaps," Rept. 634, 1938, NACA.

[3] Stevens, J. R. and McDonald, J. W., "Subsonic Lifting Surface Design and Analysis Procedure," NOR-64-195, 1965, Northrop Corp., Aircraft Div., Hawthorne, Calif.

[4] Stevens, J. R. et al., "High Lift Surface Design Procedures—Experimental Verification, Vol. I: Summary and Evaluation, Vol. II: Theoretical Design and Analysis, Vol. III: Wind Tunnel Tests," NOR 66-206, 1966, Northrop Corp., Aircraft Div., Hawthorne, Calif.

[5] Furlong, C. G. and McHugh, J. G., "A Summary and Analysis of Swept Wings at High Reynolds Number," TR 1339, 1957, NACA.